



ORIGINAL ARTICLE

One pot synthesis of chromium incorporated SBA-16 under acid medium-Application in the selective oxidation of benzyl alcohol derivatives



Zainah A. Aldhawi^{a,b}, Nuhad A. Alomair^{a,b}, Hafedh Kochkar^{a,b,*},
Chandrasekar G Revathy^b

^a Department of Chemistry, College of Science, Imam Abdulrahman Bin Faisal University, P.O. Box 1982, 31441 Dammam, Saudi Arabia

^b Basic & Applied Scientific Research Center, Imam Abdulrahman Bin Faisal University, P.O. Box 1982, 31441 Dammam, Saudi Arabia

Received 27 November 2021; accepted 23 March 2022

Available online 6 April 2022

KEYWORDS

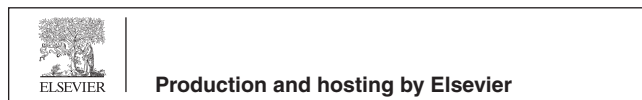
Nano-porous;
SBA-16;
Benzyl alcohol;
Noncompetitive adsorption;
Kinetics

Abstract Cr-SBA-16 mesoporous silica heterogeneous catalysts (Si/Cr = 7, 14, and 28) were successfully synthesized by one-pot hydrothermal method at low acidic medium. The catalysts were characterized by means of X-ray diffraction (XRD), N₂ adsorption-desorption at 77 K, Fourier Transform Infrared (FTIR), X-ray photoelectron (XPS) and Diffuse Reflectance UV-Vis (DRS) Spectroscopies, Thermogravimetric analysis (TGA), Scanning electron microscopy (SEM) and Transmission electron microscopy (TEM) techniques. Herein, Cr-SBA-16 catalysts are evaluated in the selective catalytic oxidation of benzyl alcohol derivatives using H₂O₂ as oxidant. From XPS and UV-Vis (DRS) spectroscopies the molar ratios between Cr⁶⁺/Cr³⁺ are found to increase versus chromium loading in the following order: Cr-SBA-16(28) < Cr-SBA-16(14) < Cr-SBA-16(7). Hence the highest Cr⁶⁺ in tetrahedrally environment is observed for Si/Cr = 7. We demonstrated for the first time that the selective catalytic oxidation of benzyl alcohol (BzOH) using H₂O₂ over Cr-SBA-16 occurs through noncompetitive adsorption mechanism and the reaction is pseudo-first order to BzOH. The activity of the reaction depends on the symmetry of chromium species, herein, high activity is observed for tetrahedral chromium species in Cr-SBA-16(7). The

* Corresponding author at: Department of Chemistry, College of Science, Imam Abdulrahman Bin Faisal University, P.O. Box 1982, 31441 Dammam, Saudi Arabia.

E-mail address: hbkochkar@iau.edu.sa (H. Kochkar).

Peer review under responsibility of King Saud University.



absence of any chromium ions in the filtrate shows no chromium leaching from the silica framework.

© 2022 The Author(s). Published by Elsevier B.V. on behalf of King Saud University. This is an open access article under the CC BY-NC-ND license (<http://creativecommons.org/licenses/by-nc-nd/4.0/>).

1. Introduction

The Catalytic oxidation process plays a vital role in both energy production /conservation, where over 90% of all chemical processes are mainly catalytic processes (Zhang et al., 2013).

Selective oxidation of primary and secondary alcohols to their carbonyl analogous (carboxylic acids, aldehydes and ketones) is of high interest in industrial organic synthesis (Chaudhary and Sharma, 2017; Ma et al., 2014). The resulted products have widespread use as intermediates in fine chemicals, pharmaceuticals, agrochemicals, and fragrance industries (Del Olmo et al., 2017; Schultz and Sigman, 2006). Traditionally, alcohols oxidation is carried out using stoichiometric metals in stoichiometric amounts such as manganese, chromium, and vanadium reagents. Nevertheless, these oxidants are corrosive, expensive, and they generate large amounts of heavy-metal waste besides their difficulties in recovery and reuse (Bahramian et al., 2006; Cordoba et al., 2017; Satrio and Doraiswamy, 2001). The increasing demand for environmentally friendly chemical processes has impelled many researchers to investigate greener systems for catalytic oxidation by means of molecular oxygen or hydrogen peroxide as oxygen source (oxidants) besides efficient recyclable catalysts (Cánepa et al., 2017). Hence, many efforts have been devoted to the selective catalytic oxidation of benzyl alcohol using H_2O_2 employing different solid catalysts.

Transition metal nanoparticles have widely used for such purpose, due to the ease of controlling its properties by varying the synthesis techniques. For example, Ragupathi et al. have been reported the synthesis of nickel aluminate (Ragupathi et al., 2017), copper aluminate (Ragupathi et al., 2014b; Ragupathi et al., 2015a), zinc aluminate (Ragupathi et al., 2014a) cobalt aluminate (Ragupathi et al., 2015b) nanoparticles by microwave combustion method (MCM) employing plants extracts. Comparing to the conventional method, the nanoparticles prepared by the microwave combustion method was found to possess enhanced structural and morphological properties led to improve their catalytic performance in the selective oxidation of benzyl alcohol.

In order to enhance the catalytic oxidation of alcohols, many researchers explored transition metals incorporation into several supports such as Co (Cordoba et al., 2017; Ragupathi et al., 2014a) bimetallic Cu-Ni (Kimi et al., 2018), Mn (Tang et al., 2009) and Cr (Thao and Nhu, 2018) into several supports to enhance the catalytic oxidation of alcohols. In the last decades, mesoporous silica materials (MSMs) were of high interest as catalyst supports due to their uniform mesoporous channel structure and high specific surface area. Among these materials' SBA-16 with its three-dimensional connected pores cage-like (cubic structure) leads to facilitate the reactants mass transfer into pores, besides its small input of pores which prevents the aggregation of metal particle (Rivera-Muñoz and Huirache-Acuña, 2010).

Numerous studies have been devoted to the catalytic oxidation of benzylic alcohol using noble metals such as Pt (Tamizhdurai et al., 2018), Pd (Chen et al., 2010b), Au (Kumar et al., 2016; Wang et al., 2015) and Ag (Cruz et al., 2016) containing mesoporous silica materials. Indeed, these catalysts remain expensive preventing their wide application. As a new alternative, the development of non-precious transition metals containing mesoporous silica materials has been investigated by several researchers. The catalytic oxidation of benzyl alcohol was explored using copper (II) complexes and copper oxide (CuO) supported onto SBA-15; 54% selectivity toward benzaldehyde is achieved at 73% conversion using H_2O_2 at 80 °C (Cruz et al., 2016). Moreover, the selective benzylic alcohol oxidation using Co, V and Fe substituted MCM-41is reported (Cánepa et al., 2017). The best catalytic performance is obtained is with V-MCM-41, 13% conversion with 100% selectivity to benzaldehyde at 70 °C. More recently, high benzyl alcohol conversion (62%) is obtained over titanium incorporated SBA-15 with Si/ Ti = 10, the selectivity to benzaldehyde reaches 96% at 60 °C in 2 h (Sharma et al., 2012). In addition, the benzyl alcohol oxidation was investigated over numerous chromium-based different materials such as Cr-loaded sepiolite (magnesium silicate) (Thao and Nhu, 2018), Cr-ZSM-5 (Lounis et al., 2006), $Cr_2O_3-Al_2O_3$ (Meng et al., 2019), doped in perovskite (Burange et al., 2013), spinel chrome M-Cr₂O₄ (Premalatha et al., 2012). Unfortunately, these catalysts are suffered from Cr leaching and low recyclability. A few reports in which chromium-containing mesoporous silica materials were applied for benzyl alcohol oxidation (Wang et al., 2007; Wang et al., 2010). Furthermore, the incorporation of transition metals into SBA-n family is a challenging step since they were synthesized under strong acidic medium where the M—O—Si bond is not stable (Zhou et al., 2018). Within this literature review, new insights for the incorporation of chromium into SBA-16 framework; to the best of our knowledge; is not yet explored. Moreover, accurate kinetic models give valuable information about the catalyst active sites, which is very useful for the catalysts and reactors design. Despite the fact the industrial relevance of this reaction and the importance of adjusting the selectivity to benzaldehyde, only a few attempts have been performed in the literature to modeling the reaction kinetics of this reaction over metals (Chaudhari and Sawant, 2005), supported metal/ metal complexes (Mahdavi et al., 2010; Mahdavi and Mardani, 2012; Rajendran et al., 2016; Zhan et al., 2013) and noble metals (Galvanin et al., 2018).

In this present study, A challenging one-pot synthesis method under low acidic medium (pH = 2) is performed for the synthesis of Cr-SBA-16 nanomaterials with different Si/ Cr molar ratios (7, 14, 28). The catalytic properties of Cr-SBA-16 are investigated in the selective oxidation of benzyl alcohol derivatives. The competitive vs noncompetitive adsorption mechanisms are applied to elucidate the benzyl alcohol reaction kinetic.

2. Experimental section

2.1. Materials

The following chemicals and reagents were used for catalyst synthesis and catalytic reaction: tetraethyl orthosilicate (TEOS) (99%), Pluronic F-127 (EO₁₀₆PO₇₀EO₁₀₆) (99%), chromium (III) nitrate nonahydrate (Cr(NO₃)₃·9H₂O) (99%) were purchased from Sigma Aldrich, n-butanol (99%) from Honywell fulka company. Benzyl alcohol (99%), benzaldehyde (99%), benzoic acid (99%), p-chlorobenzyl alcohol and p-nitrobenzyl alcohol and acetonitrile (99%) HPLC grade were purchased from Sigma Aldrich. Ultrapure water from ELGA water purification system (18 M Ω) is used through all the experiments. All chemicals were used as obtained without further purification.

2.2. Synthesis of Cr-SBA-16

The purely SBA-16 was synthesized by using the procedure described by (Zhao et al., 1998) with some modifications. In a typical synthesis, 3 g of Pluronic F127 dissolved in 145 mL HCl (0.01 M) and stirred at 45 °C. Later, 9 g of n-butanol and TEOS (14.5 g) was added to the solution dropwise under strong stirring and kept for 24 h. The final gel moved to a Teflon autoclave then aged at 100 °C for 24 h. The resulted white solid was filtered, washed with de-ionized water, dried and calcined at 550 °C. For the Cr incorporated SBA-16, a series of Cr-SBA-16(x) with different Si/Cr ratios were prepared (where x = 7, 14 and 28 ratios). The synthesis procedure of Cr-SBA-16(x) is the same as described for pure SBA-16 with only an additional step. Here, the chromium precursor (Cr(NO₃)₃·9H₂O) was added at the same time as the silica precursor (TEOS).

2.3. Catalyst characterization

The measurements of surface area and pore size by N₂-adsorption-desorption measurement at 77 K were carried out using QuantaChrome, Nova 2200e instrument equipped with QuantaChrome NovaWin software. The BET surface area (S_{BET}) was determined using the Brunauer–Emmett–Teller (BET) model through the adsorption branch data in a relative pressure P/P₀ in range of 0.050–0.3. Total porous volume (V_T) was measured at P/P₀ = 0.99. The Barret-Joyner-Halenda (BJH) model was used to obtain the pore size distribution.

X-ray diffraction analysis was carried out using Powder X-ray diffractometer Rigaku instrument by means of Cu Kα (λ = 1.54 Å) radiation with 2θ range from 0.8 to 10° with a step size of 0.02/s. Diffuse Reflectance UV–Vis Spectroscopy (DRS) measurements were performed using SHIMADZU, Solid spec-3700). The powder samples were placed on holder and the spectra were recorded in range of 200–800 nm with BaSO₄ being standard.

X-ray photoelectron spectroscopy (XPS) studies were carried out using a Thermo Scientific ESCALAB 250Xi equipped with a dual Al/Mg anode and a hemi-spherical analyzer operating at fixed pass energy of 50 eV. A 150 W monochromatic source (Al Kα = 1486.6 eV) was used to excite the samples. The samples were pressed on a double side carbon tape

attached to the sample holder and placed into the XPS instrument. Binding energies were obtained with a precision of 1.0 eV. Curve fitting was done using mixed Gaussian and Lorentzian functions (function type: product, Fitting algorithm: Powell) for line shaping after-treatment of the background using a smart type of baseline (Thermo Avantage software, version 5.51).

Scanning electron microscopy (SEM) images of samples were obtained by high-resolution field emission SEM instrument (FEI Nova NanoSEM 230) to study the morphology of samples. Transmission electron microscopy (TEM) analysis was carried out using JEM-2100F field emission microscope. Thermogravimetric analysis was carried out using TGA 2 MITTELER TOLEDO analyzer. FTIR analysis was carried out using FTIR spectroscopy (IR AFFINITY-1, Shimadzu).

2.3.1. Catalytic test

Cr-SBA-16(x) nanomaterials were investigated in the selective oxidation of benzyl alcohol derivatives. Typically, 1 mmol of benzyl alcohol and 3 mmol of 30 %v H₂O₂ (0.28 mL) were mixed with acetonitrile (20 mL) in a 50 mL two-necked round bottom flask fitted with a reflux condenser and magnetic stirrer. The resulting mixture was stirred (r = 1200 rpm) at 80 °C in an oil bath equipped with electric heater. At time zero, 30 mg of catalyst was added. Samples were removed periodically with syringe equipped with filter (0.45 μm) and analyzed by HPLC equipped with Hypersil Gold column (5 μm); using acetonitrile/water (30/70 v/v) as mobile phase and UV-visible detector (λ = 210 nm). The products were identified by comparison with standards. For the quantification of the amounts of consumed reactants and generated products, an external standard method was used.

3. Results and discussion

3.1. X-ray diffraction (XRD)

XRD of pure SBA-16 and Cr incorporated SBA-16(x) (where x = 7, 14 and 28) materials are summarized in (Fig. 1). Small angle diffraction of SBA-16 materials (Fig. 1a) displayed a strong sharp diffraction peak in the range of 0.7°–0.9° corresponding to the reflection (110), and two weak peaks at values of about 1.2° and 1.6° assigned to (200) and (211) reflections, respectively, characteristic for SBA-16 materials with three-dimensional cubic (*Im3m*) pore structure (Dong et al., 2014; Maheswari et al., 2014; Shokoohi Shooli et al., 2018). Compared to the parent SBA-16, the intensity of (110), (200) and (211) diffraction peaks of the Cr-SBA-16 materials are gradually decreased by increasing Cr-loading. This result could be attributed to the partial collapse of pore wall or due to partial blockage of the pores with increasing in Cr loading (Dong et al., 2014). As Cr loading increases in SBA-16 matrix, the main peak due to (110) reflection is shifted to lower 2θ values, indicating an increase in the lattice parameters (*d*₁₁₀-spacing and *a*₀) as shown in (Table 1). The unit cell parameter *a*₀ is 178 Å for high Cr loading (Si/Cr = 7) against 139 Å for low Cr loading (Si/Cr = 28). The increase of lattice parameters is probably due to the isomorphic substitution of Cr³⁺ with ionic radii 0.62 Å in place of Si⁴⁺ having ionic radii of 0.26 Å in the SiO₂ network. This result was explained by the length of the bond of Cr–O (Casalboni et al., 1996; Urusov

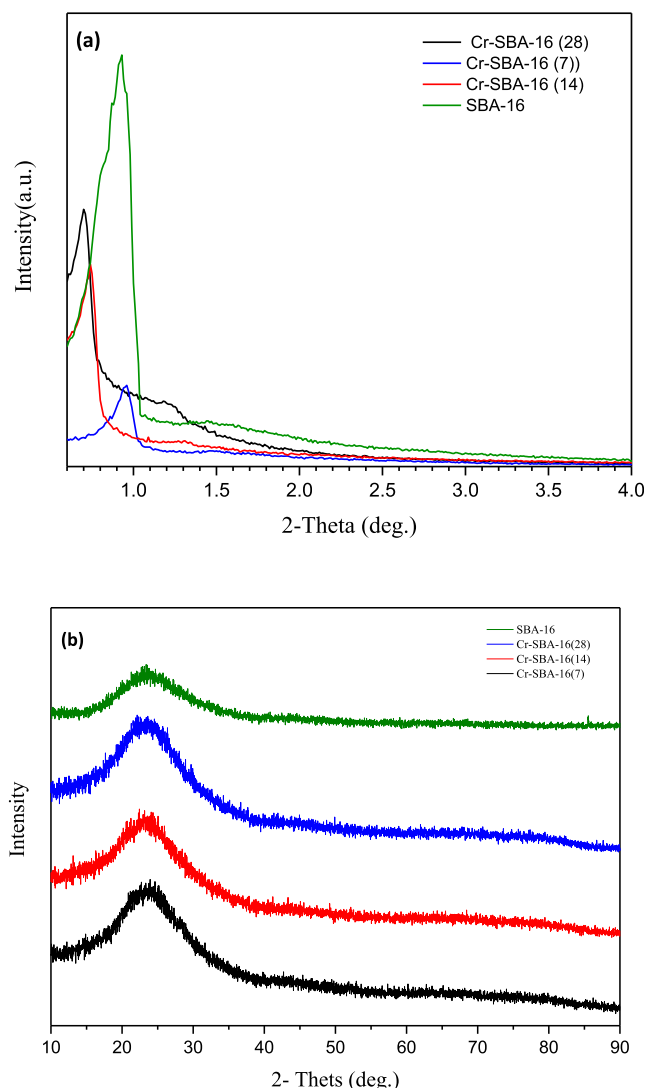


Fig. 1 a) Low-angle XRD patterns of SBA-16 and Cr-SBA-16 (x) samples and b) Wide-angle XRD of Cr-SBA-16(x) nanomaterials.

and Taran, 2012); leading to increase in the lattice parameters of Cr-SBA-16 samples compared to their free chromium SBA-16 counterpart.

See Fig. 1b, showed the wide-angle XRD patterns of Cr-SBA-16 materials. The Cr-SBA-16 samples showed a broad peak at the 2θ value of 24° attributed to amorphous silica. We noticed also the absence of any Cr_2O_3 species diffraction peaks even at high chromium loading ($\text{Si}/\text{Cr} = 7$); indicating

no agglomerated chromium oxide species onto Cr-SBA-16 samples or too small particle sizes of Cr-species.

3.2. UV-vis Diffuse Reflectance Spectroscopy

The diffuse reflectance UV-Vis spectra of SBA-16 and Cr-SBA-16 (x) are shown in (Fig. 2). Usually, the apparent color of the specimen indicates the existence of different species of metals on the samples, the green color detects the existence of trivalent chromium ions while orange or yellow color arises from the presence of hexavalent chromium species (chromate or polychromate) (Zapata et al., 2013). However, all the as-synthesized catalysts are in light green color and change into yellow color after calcination at 550°C . This result clearly shows that the former is Cr^{3+} with octahedral coordination and the latter is due to the presence of Cr^{6+} chromate and/or polychromate ions, in the tetrahedral geometry (Sakthivel and Selvam, 2002).

The pure SBA-16 shows no notable absorption in the DRS-UV-Vis spectrum suggesting that there is no d-d electronic transition in the silica sample. In the case of Cr-SBA-16 (x) samples, there are mainly two intense bands observed at 269.5 nm and 348 nm assigned to $\text{O}^{2-} \rightarrow \text{Cr}^{6+}$ charge transfer of tetrahedrally coordinated chromium oxides. These bands are attributed to ${}^1\text{A}_1 \rightarrow {}^1\text{T}_2$ transition, which indicate the presence of isolated mono-chromate species (Michorczyk and Ogonowski, 2012; Michorczyk et al., 2012; Sakthivel et al., 2001; Zhang et al., 2008). Indeed, the weak broad band around 447 nm increased gradually with an increase in chromium loading. This band is attributed to symmetry-forbidden transition ${}^1\text{A}_1 \rightarrow {}^1\text{T}_1$ is due to the existence of dichromate or polychromate species or the presence of Cr^{3+} in octahedrally coordination e.g. (Cr_2O_3) (Dragoi et al., 2013; Jourshabani et al., 2015).

3.3. X-ray photoelectron spectroscopy

The X-ray Photoelectron Spectroscopy (XPS) analysis is applied here to determine the chemical composition of the Cr-incorporated SBA-16 materials and the oxidation number of the chromium species existing therein (Fig. 3). The XPS spectra of the prepared materials consist mainly of Si 2p, O 1s and Cr 2p peaks (Fig. 3a). The XPS spectrum of the pure SBA-16 sample shows the characteristic peaks at 151.0 eV, 103.08 eV and 532.00 eV due to the binding energy of Si 2s, Si 2p and O 1s, respectively. In the Cr-SBA-16 samples, the peaks due to Si 2s, Si 2p binding energy are present. But the peak due to O1s binding energy is shifted towards lower value of 531.0 eV. This is assigned to the existence of surface lattice chromate species at the surface (Zhang et al., 2008) in good

Table 1 Textural, structural and catalytic properties of Cr-SBA-16 with different Si/Cr molar ratios (7,14,28).

Catalyst	S_{BET} (m^2/g)	V_p (cm^3/g)	d_p (\AA)	a_0 (\AA)	d_{110} (\AA)	EDX Wt%		Conversion%	Selectivity% Benzaldehyde
						Si	Cr		
SBA-16	1081	1.08	91	136	95	—	—	—	—
Cr-SBA-16 (7)	1158	1.34	75	178	126	39.95	0.16	50%	100%
Cr-SBA-16 (14)	1074	0.92	75	169	119	42.76	0.06	35.4%	100%
Cr-SBA-16 (28)	1110	1.11	75	139	98	42.3	0.35	26.4%	100%

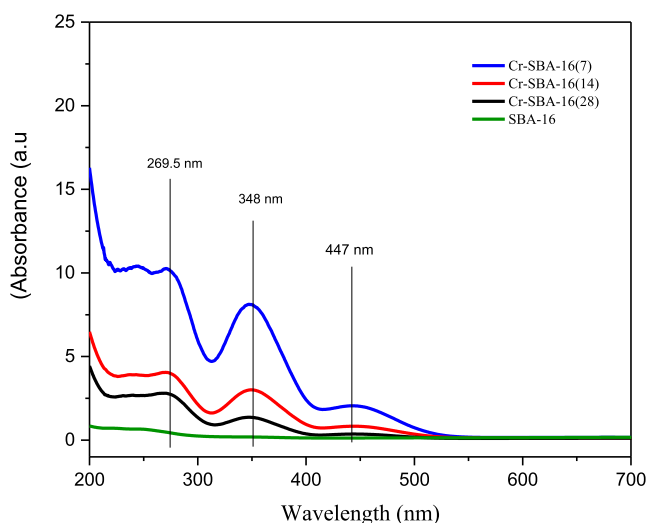


Fig. 2 DRS UV-Vis spectra of SBA-16 and Cr-SBA-16(x) nanomaterials.

agreement with DRS results. Herein, all Cr-SBA-16 (x) materials showed mainly two peaks at 585 eV and 577 eV assigned to Cr 2p_{3/2} and Cr 2p_{1/2} states, respectively (Fig. 3b-d). In order to highlight the metals species present at the surface of the catalyst, the deconvolution method is applied regarding the most intense peak 2p_{3/2} (Biesinger et al., 2011). The deconvolution of the Cr 2p_{3/2} peak shows two peaks located at 577 eV and 579 eV attributed to Cr³⁺ and Cr⁶⁺, respectively (Dragoi et al., 2013; Zhang et al., 2008).

The molar ratio between Cr⁶⁺/Cr³⁺ are estimated and found to increase versus chromium loading into SBA-16 and vary in the following order: Cr-SBA-16(28) (0.17) < Cr-SBA-16(14) (1.2) < Cr-SBA-16(7) (3.63). Hence the highest Cr⁶⁺ in tetrahedrally environment is observed for Si/Cr = 7.

3.4. Textural properties

The textural properties of the synthesized materials were investigated using N₂ adsorption-desorption measurement at 77 K (Table 1). The N₂-physisorption isotherms and corresponding pore size distributions for the Cr-SBA-16(x) samples and SBA-16 are summarized in (Fig. 4). The N₂-physisorption isotherms of pure and Cr-SBA-16(x) samples exhibit type-IV isotherms and H2 hysteresis loop with steep increase of nitrogen adsorption in P/P₀ range of 0.45–0.78, due to the capillary condensation of mesopores. This is characteristic of ordered mesoporous SBA-16 materials with 3D cage-like pore structures.

From the N₂ physisorption measurements, pure SBA-16 exhibited a high surface area (1081 m²/g), large pore diameter (90.66 Å), and high pore volume (1.08 cm³/g). The Cr incorporated materials exhibit high surface area above 1000 m²/g, (Cr-SBA-16 (7) (1158 m²/g), Cr-SBA-16 (14) (1074 m²/g) and Cr-SBA-16 (28) (1110 m²/g). The Cr-SBA-16(x) materials show slightly higher surface area than the parent SBA-16, such behavior may be hint to the expansion of unit cell parameter and indicates successful incorporation of chromium into the framework (Wang et al., 2005). These results are consistent with the low-angle XRD measurements (Table 1). Finally, the pore diameter of parent SBA-16 material decreased by

17.6% upon the incorporation of chromium in the silica lattice. However, the Cr-SBA-16(x) materials exhibit a uniform pore size distribution (average 75 Å) as illustrated in the inset of (Fig. 4).

3.5. SEM-EDX and TEM analysis

FESEM and TEM images were also acquired on the SBA-16 and Cr-SBA-16 (x) to visualize the surface morphology of the materials obtained in this study. A highly ordered arrangement of the cubic cage-like mesoporous structure of the SBA-16 and Cr-SBA-16 (x) materials is clearly visible in the TEM images (Fig. 5A, B, C, D). This result suggests successful incorporation of Cr ions without distorting the SBA-16 structure which is in good agreement with XRD results. The SEM images (Fig. 5a, b, c, d) of SBA-16 and Cr-SBA-16 (x) materials reveal that whatever the Cr loading, similar morphologies were obtained formed of rough aggregates with intergranular porosity. The effect of Cr loading on the particle size was statistically estimated using Image-J software. Results emphasize that the average particle size of SBA-16 material (15 μm) decreases versus Cr loading. The particle sizes are respectively 4.8 μm, 3.7 μm and 2.6 μm for respectively Cr-SBA-16(28), Cr-SBA-16(14) and Cr-SBA-16 (7) (Fig. 5). Therefore, it seems that the addition of chromium inhibits the SBA-16 particle growth. Otherwise, all samples show Si/Cr ratios slightly lower than the theoretical ones (Table 1). Elemental mapping, particularly for Cr, Si and O shows that their surface distribution on Cr-SB16 (x) is quite homogeneous, confirming a quite good dispersion of these elements on the surface of SBA-16 in agreement with XRD analysis. These results show homogeneous dispersion of Cr onto SBA-16 framework (Fig. 6).

3.6. FT-IR analysis

The FT-IR spectra of SBA-16, Cr-SBA-16(X) and reused Cr-SBA-16 (7) are given in (Fig. S1, supplementary information). All the absorption bands of SiO₂ are presented in all prepared and reused catalysts, indicating that the SBA-16 structure remains unchanged after Cr incorporation. The absorption bands at around 1065 cm⁻¹ and 790 cm⁻¹ are due to asymmetric and symmetric stretching vibrations of Si–O–Si, respectively. The band at about 960 cm⁻¹ is attributed to the stretching vibration of Si–O–M units (Derylo-Marczewska et al., 2006; Molaei and Ghadermazi, 2020; Molaei and Ghadermazi, 2021a,b). However, careful discretion is required to determine this band since the pure SBA-16 also exhibits such a band around 960 cm⁻¹ which is attributed to the Si–OH vibration of silanol groups that present in the mesoporous structure (Ghadermazi et al., 2021). Deep observation of spectra shows that there is an increase in the intensity of the absorption bands at 959 cm⁻¹ with increasing Cr contents. Thus, this band can be interpreted in terms of the overlapping of both Si–OH groups and Si–O–M bonds vibrations (Molaei and Ghadermazi, 2020; Shah et al., 2010).

3.7. Thermogravimetric analysis

TGA analysis (Fig. S2, supplementary information) showed higher weight loss of ca. 16% for Cr-SBA-16(28), 20% for Cr-SBA-16(14) and 23% for Cr-SBA-16 (7) between 25 and

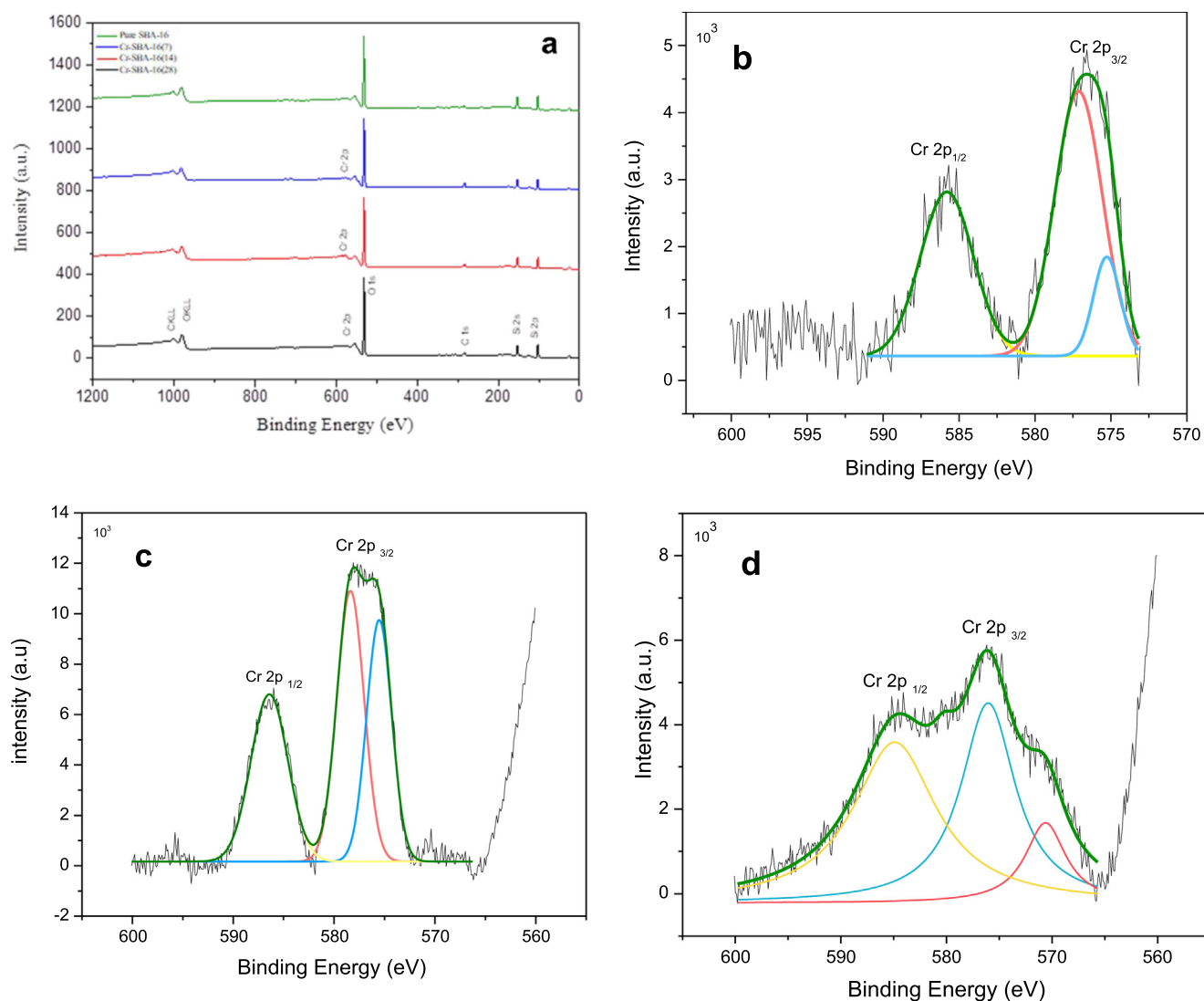


Fig. 3 a) The XPS spectra of the prepared materials consist mainly of Si 2p, O 1s and Cr 2p peaks; Cr 2p XPS spectra of b) Cr-SBA-16 (7), c) Cr-SBA-16(14) and d) Cr-SBA-16(28).

150 °C as compared to that pure SBA-16 (10%). These values are attributed to reversible dehydration and indicate higher moisture content in the Cr-SBA-16 materials compared to Cr free material. This result might be explained by possible water polarization in presence of chromium species.

3.8. Catalytic performance

3.8.1. Effect of chromium loading on catalytic properties-activation energy

The effect of Si/Cr molar ratios on the catalytic properties for selective oxidation of benzyl alcohol (BzOH) is investigated (Fig. 7). The conversion (TTG) and selectivity (TTi) are obtained using Eqs. (1) and (2):

$$\text{TTG} = \frac{C_t}{C_0 - C_t} \times 100 \quad (1)$$

$$\text{TTi} = \frac{C_i}{C_0 - C_t} \quad (2)$$

where C_0 and C_t are the initial BzOH concentration, the BzOH concentration at time $t > 0$, respectively and C_i is the product concentration.

The conversion of benzyl alcohol increases versus Cr loading (Fig. 7a). We registered 23%, 30% and 50% TTG for respectively Cr-SBA-16 (28), Cr-SBA-16 (14) and Cr-SBA-16 (7). The high TTG value for Cr-SBA-16 (7) agrees with the existence of high amount of tetrahedral Cr (VI) as identified earlier by UV-visible and XPS measurements. (Thao and Nhu, 2018) showed 30% BzOH conversion over Cr/Sepiolite catalyst using TBHP with excellent selectivity to benzaldehyde. Higher BzOH conversion is obtained (52.5%) over Cr(salen) complexes and hydrogen peroxide at 50 °C (Wang et al., 2007). The beneficial effect of the acidity of the catalyst on the BzOH conversion is showed by (Sharma et al., 2012). The same authors showed that BzOH conversion increases versus acidity of the catalyst 20% for Ti-SBA-15 against 62% for sulfated Ti-SBA-15. Metals modified MCM-41 were also applied in the selective oxidation of BzOH (Aiube et al., 2019; Canepa et al., 2017; Carrillo et al., 2013). The BzOH

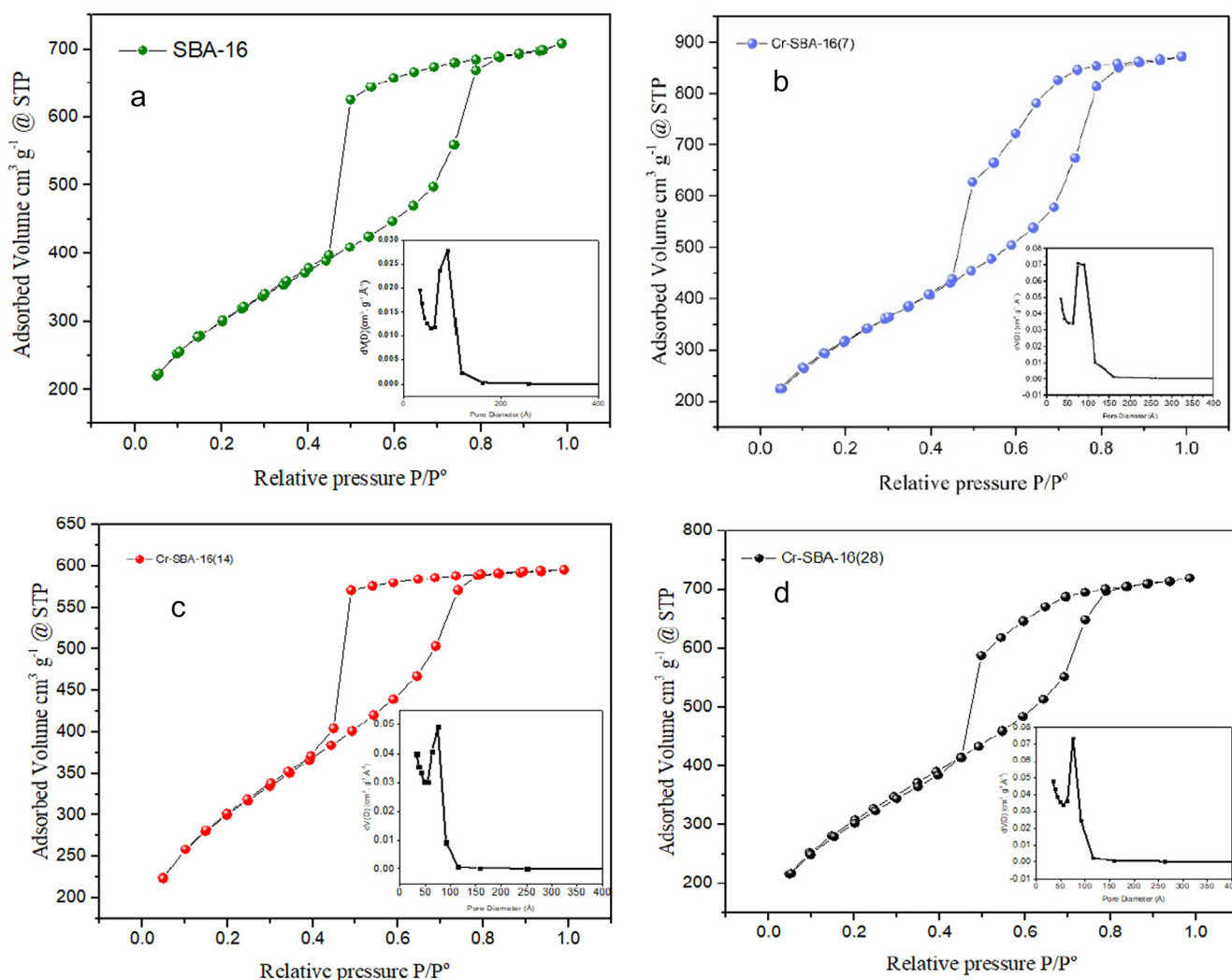


Fig. 4 N₂ adsorption–desorption measurement at 77 K of a) SBA-16, b) Cr-SBA-16(7), c) Cr-SBA-16(14) and d) Cr-SBA-16(28).

conversion was found to be vary in the following order: Fe-MCM-41 (22%) < V-MCM-41 (37%) < Ce-MCM-41 (63%). However, the highest conversion of 50% with 100% selectivity towards benzyl aldehyde are obtained using the highest tetrahedral chromium loading in Cr-SBA16(7).

In order to determine the activation energy E_a for BzOH oxidation, further studies were conducted at different temperatures (25 °C, 40 °C, 60 °C, 80 °C, and 100 °C) using Cr-SBA-16 (7) as model catalyst. According to Arrhenius equation (3).

$$k = Ae^{\frac{-E_a}{RT}} \quad (3)$$

The linear form of Arrhenius equation can be written as (4):

$$\ln(k) = \frac{-E_a}{R} \left(\frac{1}{T}\right) + \ln(A) \quad (4)$$

where k is the initial rate of the reaction, A is Arrhenius constant, R ideal gas constant (8.314 J/mol), T is temperature in Kelvin and E_a (kJ.mol⁻¹) is the activation energy. The slope of the curve in $\ln k$ vs $1/T$ gives the activation energy (E_a).

From Arrhenius plot in (Fig. S3, supplementary information), the activation energy using Cr-SBA-16 (7) catalyst was found to be 18.2 kJ.mol⁻¹. Our result is close to reported val-

ues by (Chen et al., 2010b) using Pd-Au supported onto SBA-16 catalysts. The same authors demonstrated activation energies ranging between 12.3 and 16.7 kJ.mol⁻¹, implying that the BzOH oxidation might be controlled by the diffusion of reactant molecules into the mesoporous channels. In fact, the pore size of Cr-SBA-16 (7) is large as 7.5 nm, where the diameter of the reactants and products molecules are very small (< 1 nm), which discards Yang assumption. Therefore, the effect of diffusion limitation is neglected. Moreover, the calculated activation energy is lower than that obtained by using noble monometallic or bimetallic metal supported on functionalized TUD-1(52.1 kJ.mol⁻¹) (Chen et al., 2010a), TiO₂ (45.8 kJ.mol⁻¹) (Enache et al., 2006) and TS-1 (38.2 kJ.mol⁻¹) (Zhan et al., 2013), indicating an effective Cr-SBA-16 catalyst. For comparison, (Table 2) summarizes the activation energies of different catalysts used in selective BzOH oxidation.

The conversion of BzOH increases versus temperature and reaches 50% at 80 °C (Fig. 7b). The Cr-SBA-16 seems to be more active at 100 °C, however, the conversion reaches plateau of 36% within 60 min. This could be explained by H₂O₂ decomposition at high temperatures (Chevallier et al., 2019; Han et al., 2006) or by catalyst deactivation.

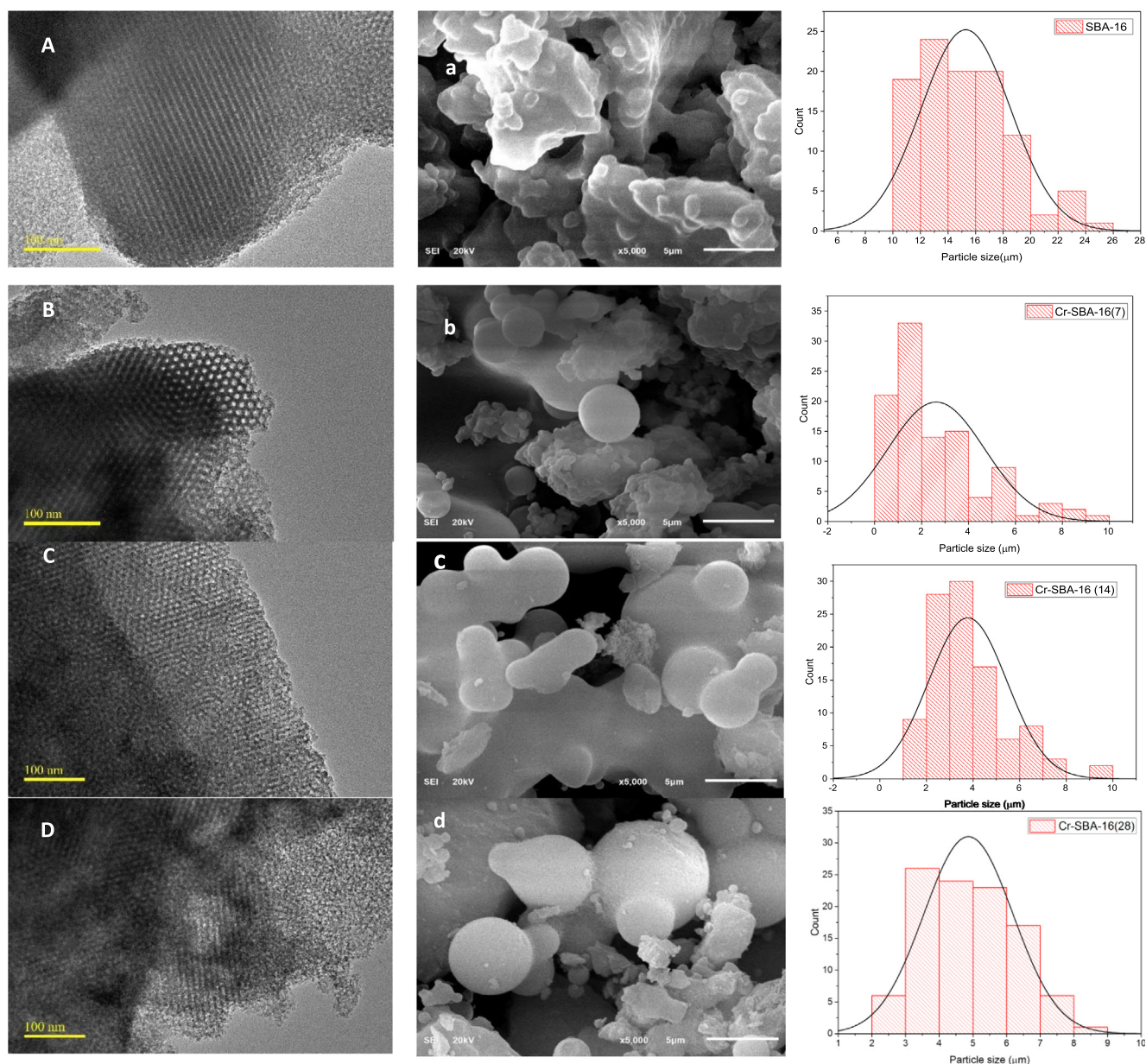


Fig. 5 TEM and SEM images of SBA-16 (A,a), Cr-SBA-16(7)(B,b), Cr-SBA-16(14) (C,c), Cr-SBA-16(28) (D,d).

3.8.2. Recyclability and leaching test

The recyclability of Cr-SBA-16 (7) catalyst was highlighted through several runs (*Fig. S4, supplementary information*). The recycling tests were conducted as follows: at the end of the reaction, the catalyst was recovered from the reaction mixture by centrifugation.

The supernatant was analyzed without any further dilution or treatment using Shimadzu AA-7000 Atomic Absorption Spectroscopy (AAS) equipped GFA-7000 graphite furnace atomizer at $\lambda = 267.7$ nm. Results emphasize the absence of any chromium leaching from silica framework. In fact, only negative absorbance values are obtained (lower than the detection limit). Hence, the selective oxidation of benzyl alcohol over Cr-SBA-16 catalyst is heterogeneous reaction.

The catalyst was thoroughly washed with (i) acetone and (ii) water, then dried at 80° overnight before being used for

the next cycle. Results indicated unchanged catalytic properties, the initial activity and TTG are almost constant. Moreover, The FT-IR spectrum (*Fig. S1, supplementary information*) and SEM images (*Fig. S5, supplementary information*) of the reused Cr-SBA-16 (7) sample indicated that structural and morphological properties remained unchanged upon 3 runs without noteworthy change in the catalyst activity.

3.8.3. Selective oxidation of benzyl alcohol derivatives

Various benzylic alcohols derivatives were subjected to oxidation over Cr-SBA-16(7) under the optimized reaction conditions (*Table 3*). The catalyst showed promising catalytic performance for benzyl alcohol derivatives oxidation. The conversion of p-chlorobenzyl alcohol and p-nitrobenzyl alcohol are 38% and 35% respectively, which is lower than the oxidation of benzyl alcohol. This result is attributed to inductive

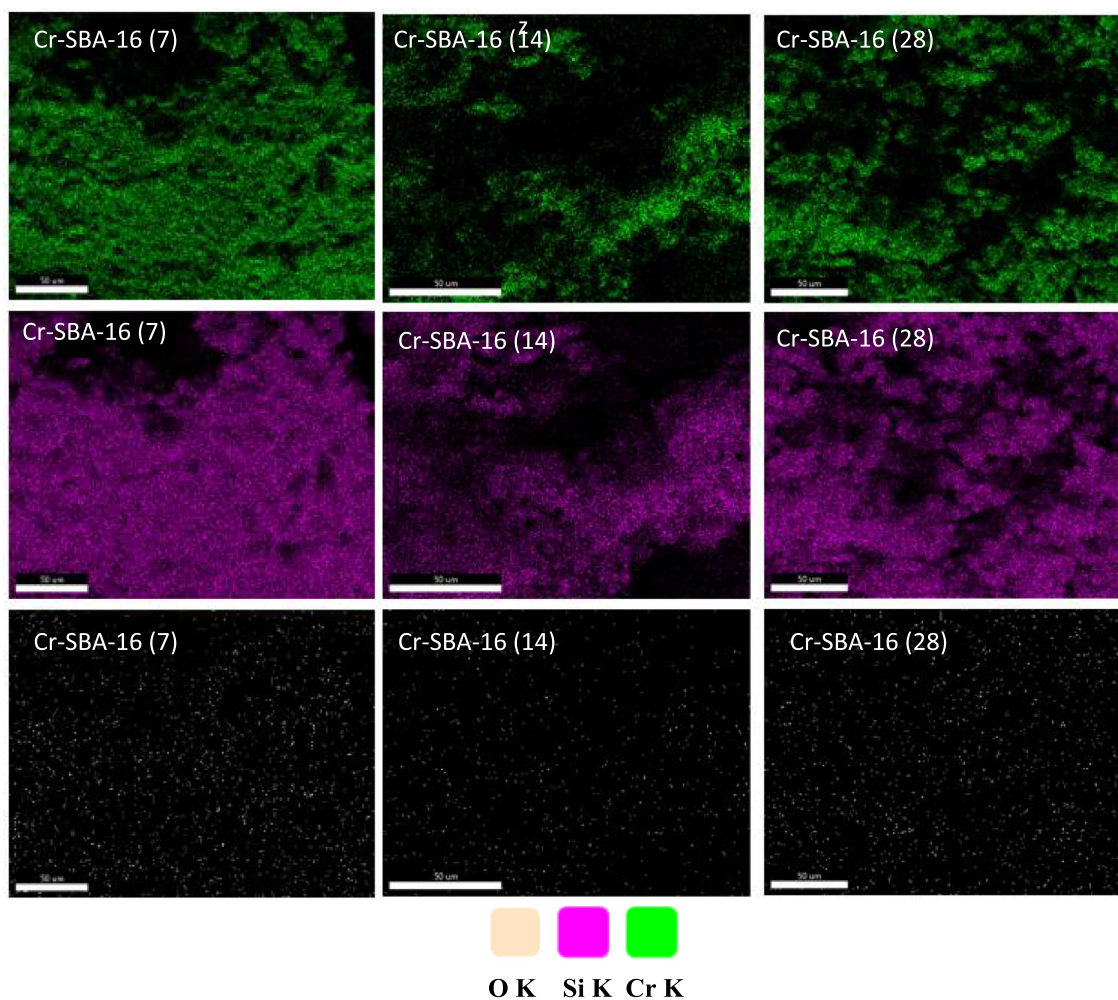


Fig. 6 Energy dispersive X-ray (EDX) mapping analysis of Cr-SBA-16 materials.

effect of the substituted groups (-chloro, -nitro). All the tested alcohols are converted to the corresponding aldehydes with 100% selectivity.

3.8.4. Kinetic studies and adsorption mechanisms

A detailed kinetic study was performed for the oxidation reaction of benzyl alcohol over Cr-SBA-16(x). Also, the effect of chromium loading on initial rate of the reaction was investigated. In order to elucidate the reaction kinetics, we modeled the experimental data using two kinetic models namely (A) pseudo-first order and (B) pseudo-second order. The rate of BzOH oxidation over Cr-SBA-16 (x) materials can be expressed by the linear form of pseudo-first order (5) and linear form of pseudo-second order (6).

$$\ln\left(\frac{[c]_t}{[c]_0}\right) = -k't \quad (5)$$

$$\frac{1}{C_t} = \frac{1}{C_0} + k''t \quad (6)$$

We can get the rate constant by plotting $\ln\left(\frac{[c]_t}{[c]_0}\right)$ versus time for pseudo-first order (k'); the slope gives the value of

pseudo-first order rate constant, and $\frac{1}{C_t}$ versus time, to obtain the pseudo-second order rate constant (k'').

Table 4 illustrates the kinetics parameters of both pseudo-first order and pseudo-second-order models. The correlation coefficient R^2 values of pseudo-first-order model are slightly higher than those of pseudo-second order model. Therefore, we can assume that the kinetic parameters of BzOH oxidation over Cr-SBA-16 catalysts are best interpreted by pseudo-first order kinetic in respect to BzOH (Fig. 8). Moreover, the pseudo-first-order rate constant k' (min^{-1}) increases versus Cr molar ratio. The variations of the initial rate versus %Cr and Cr(VI)/Cr(III) molar ratio are summarized in (Fig. 9).

The effect of Si/Cr molar ratios on the catalytic performance of benzyl alcohol oxidation is investigated. From (Fig. 9a), the catalyst with Si/Cr = 3.4 exhibits the lowest activity: we registered $0.12 \text{ mmol.L}^{-1}.\text{min}^{-1}.\text{g}^{-1}$ and $0.27 \text{ mmol.L}^{-1}.\text{min}^{-1}.\text{g}^{-1}$ for respectively Cr-SBA-16 (3.4%) and Cr-SBA-16 (12.5%). The low activity observed for Cr-SBA-16 (3.4%) agrees with the presence of low amount of tetrahedral chromium. From (Fig. 9b), the initial activity increases versus the ratio Cr(VI)/Cr(III). Therefore, the existence of Cr^{6+} is more favorable for the hydrogen peroxide adsorption than octahedral sites (Cr^{3+}), due to incomplete

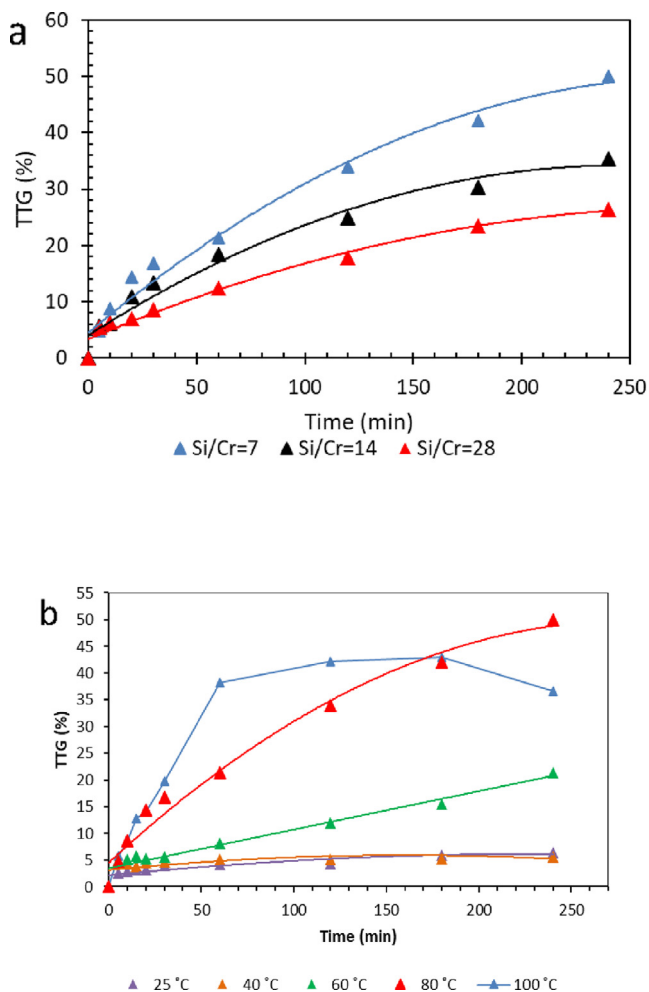


Fig. 7 a) The conversion of BzOH over Cr-SBA-16 materials and b) TTG of BzOH over Cr-SBA-16 (7) at different temperatures.

Table 2 Activation energies for BzOH oxidation using different catalysts.

Catalysts	Synthesis method	Conditions	E_a kJ.mol ⁻¹	References
Cr-SBA-16 (7)	One-pot hydrothermal	30 mg catalyst, H ₂ O ₂	18.2	This work
Pd/Co-SBA-15	Physical mixing	50 mg catalyst, O ₂	17.6	(Li et al., 2020)
Pd/Fe-SBA-15	Impregnation	50 mg catalyst, O ₂	50.08	(Li et al., 2016)
PW/MCM-41	Impregnation	150 mg, H ₂ O ₂	44.6	(Patel and Singh, 2014)
[Mn(bipy) ₂]/HMS	Impregnation	200 mg, TBHP	30.13	(Mahdavi and Mardani, 2012)
Pt/ZnO	Impregnation	100 mg, O ₂	23.7	(Liu et al., 2018)
Cobalt oxide	Mechanical mixing	200 mg, O ₂	46.14	(Ilyas and Saeed, 2010)

coordination sphere with tetrahedral Cr sites. On the other hand, the intrinsic rate of the selective oxidation of BzOH over Cr-SBA-16 materials decreases simultaneously with the Cr loading; hence, the surface area plays a minor role. For comparative reasons the pseudo rate constant of benzyl alcohol oxidation onto Sr(II)/NiAl₂O₃ (Kumar et al., 2013) and CuAl₂O₄ (Kumar et al., 2012) using (H₂O₂ or TBHP) are respectively 0.0029 min⁻¹ and 0.011 min⁻¹. Nevertheless, the comparison is quite difficult since the authors used higher amount of catalyst. Assuming that the activity (or number of active sites) is proportional to the amount of catalyst, the normalization of previous results gives 0.0867, 0.0058 and 0.011 min⁻¹/g catalyst for respectively Cr-SBA-16 (7), Sr(II)/NiAl₂O₃ and CuAl₂O₄. Hence, the best activity is obtained in this work using Cr-SBA-16 (7) catalyst.

The selective oxidation of BzOH by H₂O₂ can be described by two adsorption mechanisms using two different adsorption pathways namely: (i) competitive adsorption or (ii) non-competitive adsorption. In order to find out the best mechanism that fits with our experimental results. We will develop the two mechanisms.

First, if competitive adsorption between BzOH and H₂O₂ occurred; the occupied sites by benzyl alcohol have no accessibility to hydrogen peroxide molecules.

Therefore, the adsorption-desorption of BzOH and H₂O₂ molecules onto active sites (S) can be described by the following equations Eq. (7) and Eq. (8):



At equilibrium, the adsorption equilibrium constant for both Eq. (7) and Eq. (8) can be described respectively by Eq. (9) and Eq. (10):

$$\theta_{\text{BzOH}} = \frac{k_{\text{ads}}}{k_{\text{des}}} = \frac{[\text{BzOH} - \text{S}]}{[\text{BzOH}] \cdot [\text{S}]} \quad (9)$$

$$\theta_{\text{H}_2\text{O}_2} = \frac{k_{\text{ads}}}{k_{\text{des}}} = \frac{[\text{H}_2\text{O}_2 - \text{S}]}{[\text{H}_2\text{O}_2] \cdot [\text{S}]} \quad (10)$$

We can define the coverage of the surface by $\theta_{\text{H}_2\text{O}_2}$ and θ_{BzOH} as the ratio of occupied sites by BzOH-S or H₂O₂-S molecules to the total adsorption sites $[\alpha]_T$ Eq. (11) and Eq. (12), and the adsorption equilibrium constant $\frac{k_{\text{ads}}}{k_{\text{des}}}$ by λ for both Eq. (7) and Eq. (8):

$$\theta_{\text{BzOH}} = \frac{\text{BzOH} - \text{S}}{\sigma_T} \quad (11)$$

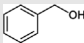
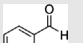
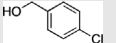
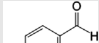
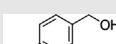
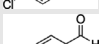
$$\theta_{\text{H}_2\text{O}_2} = \frac{\text{H}_2\text{O}_2 - \text{S}}{\sigma_T} \quad (12)$$

$$\theta_{\text{BzOH}} = \frac{\lambda_{\text{BzOH}} [\text{BzOH}]}{1 + \lambda_{\text{BzOH}} [\text{BzOH}] + \lambda_{\text{H}_2\text{O}_2} [\text{H}_2\text{O}_2]} \quad (13)$$

$$\theta_{\text{H}_2\text{O}_2} = \frac{\lambda_{\text{H}_2\text{O}_2} [\text{H}_2\text{O}_2]}{1 + \lambda_{\text{H}_2\text{O}_2} [\text{H}_2\text{O}_2] + \lambda_{\text{BzOH}} [\text{BzOH}]} \quad (14)$$

Since the reaction rate is proportional to the number of adsorbed molecules onto the surface of the catalyst ([BzOH-S] and [H₂O₂-S]). Then, the rate of the reaction will be expressed as:

Table 3 Oxidation of different benzylic alcohol over Cr-SBA-16 under the optimized conditions.

Entry	Substrate	Product	TTG (%)	Selectivity (%)
1			50%	100%
2			35%	100%
3			38%	100%

Reaction Conditions: catalyst 30 mg, alcohol (1.00 mmol) in 30 mL CH₃CN, H₂O₂ (3.00 mmol) at 80° C.

Table 4 The kinetic parameters: initial rate, pseudo-first order and pseudo-second order models of Cr-SBA-16 catalysts.

Models	Parameters	Catalysts		
		Cr-SBA-16 (7)	Cr-SBA-16 (14)	Cr-SBA-16 (28)
	% Cr (molar)	12.5	6.7	3.4
	Cr(VI)/Cr(III) (XPS)	3.6	1.2	0.17
	Initial rate (mmol. L ⁻¹ .min ⁻¹ .g ⁻¹)	0.27	0.15	0.12
Pseudo-first order	k' (min ⁻¹)	0.0030	0.0017	0.0012
	R ²	0.9939	0.9952	0.9987
Pseudo-second order	k'' (mmol ⁻¹ Lmin ⁻¹)	0.0042	0.0022	0.0015
	R ²	0.9396	0.975	0.975

$$r = q[BzOH - S] \cdot [H_2O_2 - S] \quad (15)$$

where the q is the rate constant, and by combining Eq. (13) and Eq. (14) with Eq.(15) gives:

$$r = q(\alpha_T)2\theta_{BzOH} \cdot \theta_{H_2O_2} \quad (16)$$

The α_T is proportional to the catalyst weight (m), the rate of the reaction can define as:

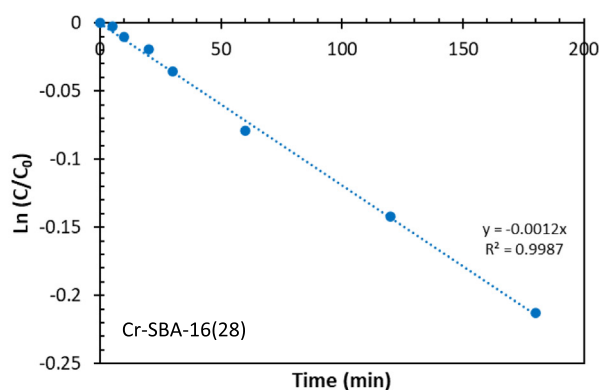
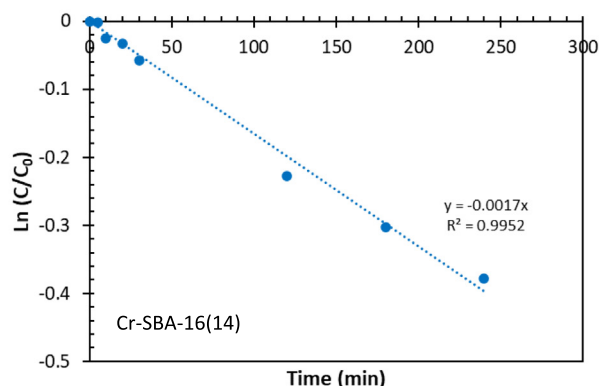
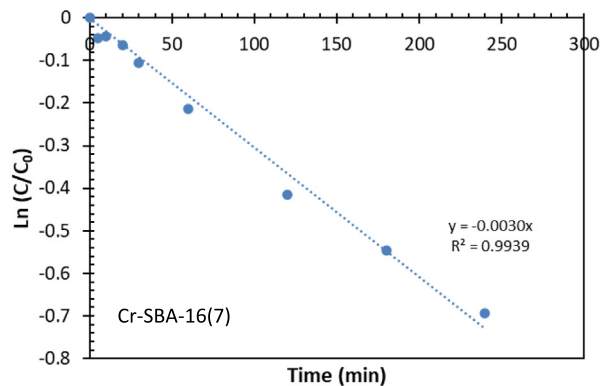
$$r' = \frac{r}{m} = \frac{qS_T^2}{m} \theta_{BzOH} \cdot \theta_{H_2O_2} \quad (17)$$

$$r' = K\theta_{BzOH} \cdot \theta_{H_2O_2} \quad (K : \text{is } \frac{qS_T^2}{m}, \text{ the rate constant}) \quad (18)$$

From Eq. (13) and (14) the expressions of θ_{BzOH} $\theta_{H_2O_2}$ are introduced in Eq. (19) gives:

$$r' = K \frac{\lambda_{BzOH} [BzOH] \lambda_{H_2O_2} [H_2O_2]}{(1 + \lambda_{BzOH} [BzOH] + \lambda_{H_2O_2} [H_2O_2])^2} \quad (19)$$

With respect to benzyl alcohol, we can assume that H₂O₂ (most polar) will be highly absorbed onto the hydroxyl groups of SBA-16 (surface defects). This hypothesis could be described by the creation of hydrogen bonds between free silanol groups and hydrogen peroxide molecule (Lewandowski et al., 2014) and/or chromium hydroxyl of chromate. As first consequence, $\lambda_{H_2O_2} \gg \lambda_{BzOH}$ and the rate of the reaction can be simplified as Eq.(20):

**Fig. 8** The pseudo first order (A) and pseudo second order plots of Cr-SBA-16 materials.

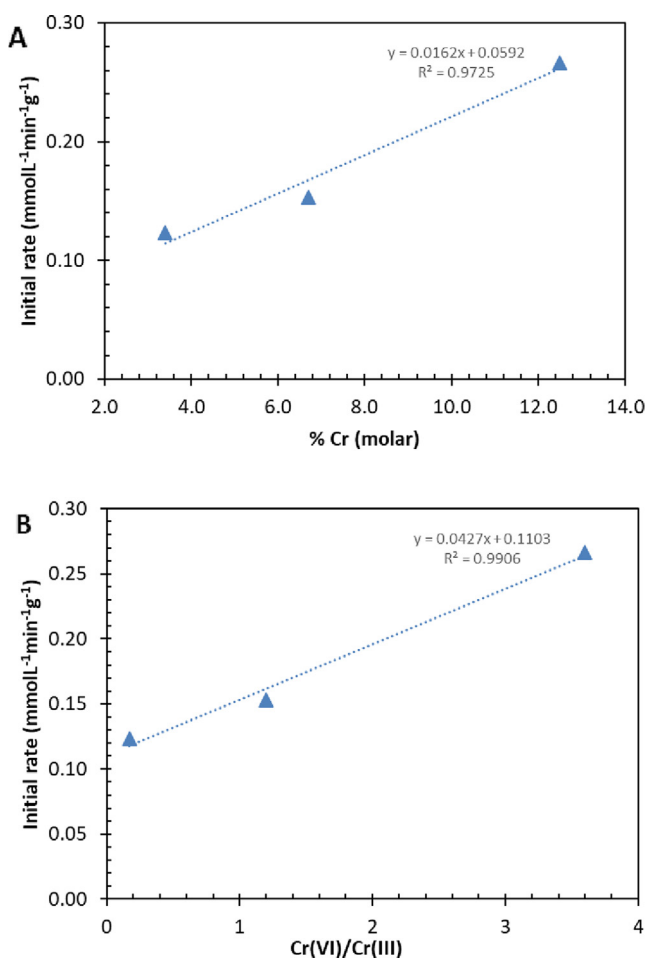


Fig. 9 a) Initial rate vs Cr loading (A) and b) Initial rate vs Cr (VI)/Cr(III) molar ratio from XPS.

$$r' = K \frac{\lambda_{BzOH} [BzOH]}{\lambda_{H_2O_2} [H_2O_2]} \quad (20)$$

Here we can conclude that the reaction has first order to BzOH and -1 order to the hydrogen peroxide. This means the hydrogen peroxide is massively occupied the surface of the catalysts and prevents the BzOH adsorption, as a result, poor catalytic properties will be obtained. This assumption does not match with our experimental results, high BzOH conversion is obtained with our Cr-SBA-16 catalysts. Then we can rule out the competitive adsorption mechanism. Thus, a non-competitive adsorption mechanism was explored also. Here, the adsorption of BzOH and H_2O_2 occurs on different active sites. Thus, the equations of the θ_{BzOH} and $\theta_{H_2O_2}$ become:

$$\theta_{BzOH} = \frac{\lambda_{BzOH} [BzOH]}{1 + \lambda_{BzOH} [BzOH]} \quad (21)$$

$$\theta_{H_2O_2} = \frac{\lambda_{H_2O_2} [H_2O_2]}{1 + \lambda_{H_2O_2} [H_2O_2]} \quad (22)$$

As previously the rate of reaction will be written as follows:

$$r' = K \frac{\lambda_{BzOH} [BzOH]}{1 + \lambda_{BzOH} [BzOH]} \times \frac{\lambda_{H_2O_2} [H_2O_2]}{1 + \lambda_{H_2O_2} [H_2O_2]} \quad (23)$$

Since $\lambda_{H_2O_2} \gg \lambda_{BzOH}$ and since we are using an excess of H_2O_2 ($1 \ll \lambda_{H_2O_2} [H_2O_2]$).

$$\theta_{H_2O_2} = \frac{\lambda_{H_2O_2} [H_2O_2]}{1 + \lambda_{H_2O_2} [H_2O_2]} = \frac{\lambda_{H_2O_2} [H_2O_2]}{\lambda_{H_2O_2} [H_2O_2]} = 1 \quad (24)$$

The rate of the reaction becomes:

$$r' = K \lambda_{BzOH} [BzOH] = k' [BzOH] \quad (25)$$

From Eq. (25) the reaction is pseudo first order in respect to benzyl alcohol, we can conclude, this assumption fits well with our experimental data (Fig. 8 and Table 4). Thus, the benzyl alcohol oxidation reaction over chromium catalysts follows a non-competitive adsorption mechanism.

4. Conclusion

In summary, an efficient ordered Cr incorporated SBA-16 was successively synthesized under weak acidic medium for selective benzyl alcohol oxidation under mild conditions. A detailed kinetic study has been performed; Non-competitive adsorption mechanism between benzyl alcohol and hydrogen peroxide is developed. The reaction was found to follow pseudo-first order model in respect to BzOH. The symmetry of Cr species present in the catalyst plays an important role in the catalytic performance. Herein, higher selectivity to benzaldehyde is reached at 50% conversion over Cr-SBA-16(7). The obtained activation energy ($18.2 \text{ kJ}\cdot\text{mol}^{-1}$) implies that the BzOH oxidation might be controlled by the diffusion of reactant molecules into the mesoporous channels. These catalysts are very effective for the selective oxidation of benzyl alcohol derivatives.

Declaration of Competing Interest

The authors declare that they have no known competing financial interests or personal relationships that could have appeared to influence the work reported in this paper.

Acknowledgement

The authors would like to acknowledge the fundings from Imam Abdulrahman Bin Faisal University, Basic and Applied Scientific Research Center obtained and Deputyship for Research & Innovation, Saudi Arabia : DSR-2019-087 Sci and IF-2020-19-BASRC.

Appendix A. Supplementary data

Supplementary data to this article can be found online at <https://doi.org/10.1016/j.arabjc.2022.103861>.

References

- Aiube, C.M., Oliveira, K.V.D., & Macedo, J.L.D., 2019. Effect of cerium precursor in the synthesis of Ce-MCM-41 and in the efficiency for liquid-phase oxidation of benzyl alcohol. *Catalysts* 9 (4), 377. [10.3390/catal9040377](https://doi.org/10.3390/catal9040377).
- Bahramian, B., Mirkhani, V., Moghadam, M., Amin, A.H., 2006. Water-soluble manganese (III) salen complex as a mild and selective catalyst for oxidation of alcohols. *Appl. Catal. A: General* 315, 52–57. <https://doi.org/10.1016/j.apcata.2006.08.037>.
- Biesinger, M.C., Payne, B.P., Grosvenor, A.P., Lau, L.W., Gerson, A. R., Smart, R.S.C., 2011. Resolving surface chemical states in XPS analysis of first row transition metals, oxides and hydroxides: Cr,

- Mn, Fe, Co and Ni. *Appl. Surface Sci.* 257 (7), 2717–2730. <https://doi.org/10.1016/j.apsusc.2010.10.051>.
- Burange, A.S., Jayaram, R.V., Shukla, R., Tyagi, A.K., 2013. Oxidation of benzylic alcohols to carbonyls using tert-butyl hydroperoxide over pure phase nanocrystalline CeCrO₃. *Catal. Commun.* 40, 27–31. <https://doi.org/10.1016/j.catcom.2013.05.019>.
- Cánepa, A.L., Elías, V.R., Vaschetti, V.M., Sabre, E.V., Eimer, G.A., Casuscelli, S.G., 2017. Selective oxidation of benzyl alcohol through eco-friendly processes using mesoporous V-MCM-41, Fe-MCM-41 and Co-MCM-41 materials. *Appl. Catal. A: General* 545, 72–78. <https://doi.org/10.1016/j.apcata.2017.07.039>.
- Carrillo, A.I., Serrano, E., Luque, R., García-Martínez, J., 2013. Microwave-assisted catalysis by iron oxide nanoparticles on MCM-41: effect of the support morphology. *Appl. Catal. A: General* 453, 383–390. <https://doi.org/10.1016/j.apcata.2012.12.041>.
- Casalboni, M., Ciafardone, V., Giuli, G., Izzi, B., Paris, E., Proposito, P., 1996. An optical study of silicate glass containing and ions. *J. Phys.: Condens. Matter* 8 (46), 9059. <https://doi.org/10.1088/0953-8984/8/46/011>.
- Chaudhari, M.P., Sawant, S.B., 2005. Kinetics of heterogeneous oxidation of benzyl alcohol with hydrogen peroxide. *Chem. Eng. J.* 106 (2), 111–118. <https://doi.org/10.1016/j.cej.2004.07.014>.
- Chaudhary, V., Sharma, S., 2017. An overview of ordered mesoporous material SBA-15: synthesis, functionalization and application in oxidation reactions. *J. Porous Mater.* 24 (3), 741–749. <https://doi.org/10.1007/s10934-016-0311-z>.
- Chen, Y., Guo, Z., Chen, T., Yang, Y., 2010a. Surface-functionalized TUD-1 mesoporous molecular sieve supported palladium for solvent-free aerobic oxidation of benzyl alcohol. *J. Catal.* 275 (1), 11–24. <https://doi.org/10.1016/j.jcat.2010.07.006>.
- Chen, Y., Lim, H., Tang, Q., Gao, Y., Sun, T., Yan, Q., Yang, Y., 2010b. Solvent-free aerobic oxidation of benzyl alcohol over Pd monometallic and Au–Pd bimetallic catalysts supported on SBA-16 mesoporous molecular sieves. *Appl. Catal. A: General* 380 (1–2), 55–65. <https://doi.org/10.1016/j.apcata.2010.03.026>.
- Chevallier, M.L., Dessolin, S., Serres, F., Bruyas, L., Chatel, G., 2019. Effect of ultrasound on the green selective oxidation of benzyl alcohol to benzaldehyde. *Molecules* 24 (22), 4157. <https://doi.org/10.3390/molecules24224157>.
- Cordoba, M., Miranda, C., Lederhos, C., Coloma-Pascual, F., Ardila, A., Fuentes, G.A., Ramírez, A., 2017. Catalytic performance of Co₃O₄ on different activated carbon supports in the benzyl alcohol oxidation. *Catalysts* 7 (12), 384. <https://doi.org/10.3390/catal7120384>.
- Cruz, P., Perez, Y., del Hierro, I., Fajardo, M., 2016. Copper, copper oxide nanoparticles and copper complexes supported on mesoporous SBA-15 as catalysts in the selective oxidation of benzyl alcohol in aqueous phase. *Microporous Mesoporous Mater.* 220, 136–147. <https://doi.org/10.1016/j.micromeso.2015.08.029>.
- Del Olmo, A., Calzada, J., Nuñez, M., 2017. Benzoic acid and its derivatives as naturally occurring compounds in foods and as additives: Uses, exposure, and controversy. *Crit. Rev. Food Sci. Nutr.* 57 (14), 3084–3103. <https://doi.org/10.1080/10408398.2015.1087964>.
- Derylo-Marczewska, A., Gac, W., Popivnyak, N., Zukocinski, G., Pasieczna, S., 2006. The influence of preparation method on the structure and redox properties of mesoporous Mn-MCM-41 materials. *Catal. Today* 114 (2–3), 293–306. <https://doi.org/10.1016/j.cattod.2006.02.066>.
- Dong, Y., Zhan, X., Niu, X., Li, J., Yuan, F., Zhu, Y., Fu, H., 2014. Facile synthesis of Co-SBA-16 mesoporous molecular sieves with EISA method and their applications for hydroxylation of benzene. *Microporous Mesoporous Mater.* 185, 97–106. <https://doi.org/10.1016/j.micromeso.2013.09.037>.
- Dragoi, B., Ungureanu, A., Chiriac, A., Hulea, V., Royer, S., Dumitriu, E., 2013. Enhancing the performance of SBA-15-supported copper catalysts by chromium addition for the chemoselective hydrogenation of trans-cinnamaldehyde. *Catal. Sci. Technol.* 3 (9), 2319–2329. <https://doi.org/10.1039/c3cy00198a>.
- Enache, D.I., Edwards, J.K., Landon, P., Solsona-Espriu, B., Carley, A.F., Herzing, A.A., Hutchings, G.J., 2006. Solvent-free oxidation of primary alcohols to aldehydes using Au-Pd/TiO₂ catalysts. *Science* 311 (5759), 362–365. <https://doi.org/10.1126/science.1120560>.
- Galvanin, F., Sankar, M., Cattaneo, S., Bethell, D., Dua, V., Hutchings, G.J., Gavriilidis, A., 2018. On the development of kinetic models for solvent-free benzyl alcohol oxidation over a gold-palladium catalyst. *Chem. Eng. J.* 342, 196–210. <https://doi.org/10.1016/j.cej.2017.11.165>.
- Ghadermazi, M., Molaei, S., Ghadermazi, N., 2021. Introduction of Fe into mesoporous MCM-41 for the synthesis of 5-substituted 1H-Tetrazoles from aryl nitriles in water. *Microporous Mesoporous Mater.* 328,. <https://doi.org/10.1016/j.micromeso.2021.111441>.
- Han, H., Zhang, S., Hou, H., Fan, Y., Zhu, Y., 2006. Fe (Cu)-Containing Coordination Polymers: Syntheses, Crystal Structures, and Applications as Benzyl Alcohol Oxidation Catalysts. In: Wiley Online Library.
- Ilyas, M., Saeed, M., 2010. *Oxidation of Benzyl Alcohol in Liquid Phase Catalyzed by Cobalt Oxide*. *Int. J. of Chem. React. Eng.* 8, A77.
- Jourshabani, M., Badii, A., Lashgari, N., Ziarani, G.M., 2015. Highly selective production of phenol from benzene over mesoporous silica-supported chromium catalyst: Role of response surface methodology in optimization of operating variables. *Chin. J. Catal.* 36 (11), 2020–2029. [https://doi.org/10.1016/s1872-2067\(15\)60898-1](https://doi.org/10.1016/s1872-2067(15)60898-1).
- Kimi, M., Jaidie, M.M.H., Pang, S.C., 2018. Bimetallic Cu-Ni nanoparticles supported on activated carbon for catalytic oxidation of benzyl alcohol. *J. Phys. Chem. Solids* 112, 50–53. <https://doi.org/10.1016/j.jpcs.2017.09.008>.
- Kumar, A., Kumar, V.P., Srikanth, A., Vishwanathan, V., Chary, K. V.R., 2016. Vapor phase oxidation of benzyl alcohol over nano Au/SBA-15 catalysts: effect of preparation methods. *Catal. Lett.* 146 (1), 35–46. <https://doi.org/10.1007/s10562-015-1656-7>.
- Kumar, R.T., Suresh, P., Selvam, N.C.S., Kennedy, L.J., Vijaya, J.J., 2012. Comparative study of nano copper aluminate spinel prepared by sol-gel and modified sol-gel techniques: structural, electrical, optical and catalytic studies. *J. Alloy. Compd.* 522, 39–45. <https://doi.org/10.1016/j.jallcom.2012.01.064>.
- Kumar, R.T., Vijaya, J.J., Kennedy, L.J., 2013. Modified sol-gel prepared Sr (II)-added nickel aluminate nanocatalysts for selective oxidation of benzyl alcohol. *J. Nanosci. Nanotechnol.* 13 (4), 2953–2960. <https://doi.org/10.1166/jnn.2013.7337>.
- Lewandowski, D., Bajerlein, D., Schroeder, G., 2014. Adsorption of hydrogen peroxide on functionalized mesoporous silica surfaces. *Struct. Chem.* 25 (5), 1505–1512. <https://doi.org/10.1007/s11224-014-0428-0>.
- Li, Y., Chatterjee, A., Chen, L.B., Leung-YukLam, F., Hu, X., 2020. Pd doped Co functionalized SBA-15 as an active magnetic catalyst for low temperature solventless additive-base-free selective oxidation of benzyl alcohol. *Molecular Catalysis* 488, 110869. <https://doi.org/10.1016/j.mcat.2020.110869>. In this issue.
- Li, Y., Huang, J., Hu, X., Leung-YukLama, F., Wang, W., Luque, R., 2016. Heterogeneous Pd catalyst for mild solvent-free oxidation of benzyl alcohol. *Journal of Molecular Catalysis A: Chemical* 425, 61–67. <https://doi.org/10.1016/j.molcata.2016.09.030>. In this issue.
- Liu, J., Zou, S., Wu, J., Kobayashi, H., Zhao, H., Fan, J., 2018. Green catalytic oxidation of benzyl alcohol over Pt/ZnO in base-free aqueous medium at room temperature. *Chinese Journal of Catalysis* 39, 1081–1089. [https://doi.org/10.1016/S1872-2067\(18\)63022-0](https://doi.org/10.1016/S1872-2067(18)63022-0). In this issue.
- Lounis, Z., Riahi, A., Djafri, F., Muzart, J., 2006. Chromium-exchanged zeolite (CrE-ZSM-5) as catalyst for alcohol oxidation and benzylic oxidation with t-BuOOH. *Appl. Catal. A: General* 309 (2), 270–272. <https://doi.org/10.1016/j.apcata.2006.05.015>.

- Ma, L., Guo, X., Xiang, L., 2014. Catalytic activity of Ag/SBA-15 for low-temperature gas-phase selective oxidation of benzyl alcohol to benzaldehyde. *Chin. J. Catal.* 35 (1), 108–119. [https://doi.org/10.1016/s1872-2067\(12\)60720-7](https://doi.org/10.1016/s1872-2067(12)60720-7).
- Mahdavi, V., Hasheminasab, H.R., Abdollahi, S., 2010. Liquid phase selective oxidation of alcohols over VPO catalysts supported on mesoporous Hexagonal Molecular Sieves (HMS). *J. Chin. Chem. Soc.* 57 (2), 189–198. <https://doi.org/10.1002/jccs.201000030>.
- Mahdavi, V., Mardani, M., 2012. Selective oxidation of benzyl alcohol with tert-butylhydroperoxide catalysed via Mn (II) 2, 2-bipyridine complexes immobilized over the mesoporous hexagonal molecular sieves (HMS). *J. Chem. Sci.* 124 (5), 1107–1115. <https://doi.org/10.1007/s12039-012-0307-4>.
- Maheswari, R., Pachamuthu, M.P., Ramanathan, A., Subramaniam, B., 2014. Synthesis, characterization, and epoxidation activity of tungsten-incorporated SBA-16 (W-SBA-16). *Ind. Eng. Chem. Res.* 53 (49), 18833–18839. <https://doi.org/10.1021/ie501784c>.
- Meng, S., Chang, S., Chen, S., 2019. Synergistic effect of photocatalyst CdS and thermalcatalyst Cr2O3-Al2O3 for selective oxidation of aromatic alcohols into corresponding aldehydes. *ACS Appl. Mater. Interfaces* 12 (2), 2531–2538. <https://doi.org/10.1021/acsami.9b19473>.
- Michorczyk, P., Ogonowski, J., 2012. In situ UV-Vis DRS evidence of Cr 2+ species oxidation by CO 2. *Chem. Commun.* 48 (58), 7283–7285. <https://doi.org/10.1039/c2cc32056h>.
- Michorczyk, P., Pietrzyk, P., Ogonowski, J., 2012. Preparation and characterization of SBA-1–supported chromium oxide catalysts for CO2 assisted dehydrogenation of propane. *Microporous Mesoporous Mater.* 161, 56–66. <https://doi.org/10.1016/j.micromeso.2012.05.011>.
- Molaei, S., Ghadermazi, M., 2020. Highly ordered mesoporous La (III)-substituted 5-oxopyrrolidine-2-carboxylic acid (Glp) immobilized on SBA-15 as a very efficient nanocatalyst for green aerobic oxidative coupling of thiols to disulfides. *Appl. Organomet. Chem.* 34, (2). <https://doi.org/10.1002/aoc.5328> e5328.
- Molaei, S., Ghadermazi, M., 2021a. A green methodology for thioether formation reaction and synthesis of symmetrical disulfides over new heterogeneous Cu attached to bifunctionalized mesoporous MCM-41. *Microporous Mesoporous Mater.* 319. <https://doi.org/10.1016/j.micromeso.2021.110990> 110990.
- Molaei, S., Ghadermazi, M., 2021b. Cu attached functionalized mesoporous MCM-41: a novel heterogeneous nanocatalyst for eco-friendly one-step thioether formation reaction and synthesis of 5-substituted 1H-tetrazoles. *Res. Chem. Intermed.* 47, 4557–4581. <https://doi.org/10.1007/s11164-021-04543-2>.
- Patel, A., Singh, S., 2014. Undecatungstophosphate anchored to MCM-41: An ecofriendly and efficient bifunctional solid catalyst for non-solvent liquid-phase oxidation as well as esterification of benzyl alcohol. *Microporous Mesoporous Mater.* 195, 240–249. <https://doi.org/10.1016/j.micromeso.2014.04.039>.
- Premalatha, K., Raghavan, P., Viswanathan, B., 2012. Liquid phase oxidation of benzyl alcohol with molecular oxygen catalyzed by metal chromites. *Appl. Catal. A: General* 419, 203–209. <https://doi.org/10.1016/j.apcata.2012.01.028>.
- Ragupathi, C., Kennedy, L.J., Vijaya, J.J., 2014a. A new approach: Synthesis, characterization and optical studies of nano-zinc aluminate. *Adv. Powder Technol.* 25 (1), 267–273. <https://doi.org/10.1016/j.apt.2013.04.013>.
- Ragupathi, C., Vijaya, J.J., Kennedy, L.J., 2017. Preparation, characterization and catalytic properties of nickel aluminate nanoparticles: A comparison between conventional and microwave method. *J. Saudi Chem. Soc.* 21, S231–S239. <https://doi.org/10.1016/j.jscs.2014.01.006>.
- Ragupathi, C., Vijaya, J.J., Kennedy, L.J., Bououdina, M., 2014b. Nanostructured copper aluminate spinels: Synthesis, structural, optical, magnetic, and catalytic properties. *Mater. Sci. Semicond. Process.* 24, 146–156. <https://doi.org/10.1016/j.mssp.2014.03.026>.
- Ragupathi, C., Vijaya, J.J., Kumar, R.T., Kennedy, L.J., 2015a. Selective liquid phase oxidation of benzyl alcohol catalyzed by copper aluminate nanostructures. *J. Mol. Struct.* 1079, 182–188. <https://doi.org/10.1016/j.molstruc.2014.09.045>.
- Ragupathi, C., Vijaya, J.J., Narayanan, S., Jesudoss, S., Kennedy, L. J., 2015b. Highly selective oxidation of benzyl alcohol to benzaldehyde with hydrogen peroxide by cobalt aluminate catalysis: a comparison of conventional and microwave methods. *Ceram. Int.* 41 (2), 2069–2080. <https://doi.org/10.1016/j.ceramint.2014.10.002>.
- Rajendran, P., Divya, T., Bashpa, P., Bijudas, K., 2016. Kinetics of oxidation of benzyl alcohol by molecular oxygen using manganese oxide supported activated carbon with phase transfer catalyst. *J. Chem. Pharmaceut. Sci.* 22–27. <https://doi.org/10.1002/kin.20922>.
- Rivera-Muñoz, E.M., Huirache-Acuña, R., 2010. Sol gel-derived SBA-16 mesoporous material. *Int. J. Mol. Sci.* 11 (9), 3069–3086. <https://doi.org/10.3390/ijms11093069>.
- Sakthivel, A., Dapurkar, S.E., Selvam, P., 2001. Mesoporous (Cr) MCM-41 and (Cr) MCM-48 molecular sieves: promising heterogeneous catalysts for liquid phase oxidation reactions. *Catal. Lett.* 77 (1), 155–158. <https://doi.org/10.1039/b301899g>.
- Sakthivel, A., Selvam, P., 2002. Mesoporous (Cr) MCM-41: A mild and efficient heterogeneous catalyst for selective oxidation of cyclohexane. *J. Catal.* 211 (1), 134–143. <https://doi.org/10.1006/jcat.2002.3711>.
- Satrio, J.A., Doraiswamy, L., 2001. Production of benzaldehyde: a case study in a possible industrial application of phase-transfer catalysis. *Chem. Eng. J.* 82 (1–3), 43–56. [https://doi.org/10.1016/s1385-8947\(00\)00351-x](https://doi.org/10.1016/s1385-8947(00)00351-x).
- Schultz, M.J., Sigman, M.S., 2006. Recent advances in homogeneous transition metal-catalyzed aerobic alcohol oxidations. *Tetrahedron* 35 (62), 8227–8241. <https://doi.org/10.1016/j.tet.2006.06.065>.
- Shah, A.T., Li, B., Abdalla, Z.E.A., 2010. Direct synthesis of Cu-SBA-16 by internal pH-modification method and its performance for adsorption of dibenzothiophene. *Microporous Mesoporous Mater.* 130 (1–3), 248–254. <https://doi.org/10.1016/j.micromeso.2009.11.017>.
- Sharma, R.V., Soni, K.K., Dalai, A.K., 2012. Preparation, characterization and application of sulfated Ti-SBA-15 catalyst for oxidation of benzyl alcohol to benzaldehyde. *Catal. Commun.* 29, 87–91. <https://doi.org/10.1016/j.catcom.2012.09.027>.
- Shokoohi Shooli, Z., Izadbakhsh, A., Sanati, A.M., 2018. Effect of cerium and cerium on the performance of Ni-SBA-16 in the partial oxidation of methane. *Reaction Kinetics, Mech. Catal.* 124 (2), 873–889. <https://doi.org/10.1007/s11144-018-1375-3>.
- Tamizhdurai, P., Sakthinathan, S., Krishnan, P.S., Ramesh, A., Abilarasu, A., Mangesh, V., Chiu, T.-W., 2018. Highly selective oxidation of benzyl alcohol over Pt-sulphated zirconia supported on SBA-15 catalyst by using a high-pressure fixed bed reactor. *Polyhedron* 155, 390–397. <https://doi.org/10.1016/j.poly.2018.08.053>.
- Tang, Q., Gong, X., Wu, C., Chen, Y., Borgna, A., Yang, Y., 2009. Insights into the nature of alumina-supported MnOOH and its catalytic performance in the aerobic oxidation of benzyl alcohol. *Catal. Commun.* 10 (7), 1122–1126. <https://doi.org/10.1016/j.catcom.2009.01.011>.
- Thao, N.T., Nhu, N.T., 2018. Evaluation of catalytic activity of MeOx/sepiolite in benzyl alcohol oxidation. *J. Sci.: Adv. Mater. Devices* 3 (3), 289–295. <https://doi.org/10.1016/j.jsamd.2018.07.006>.
- Urusov, V.S., Taran, M.N., 2012. Structural relaxation and crystal field stabilization in Cr3+-containing oxides and silicates. *Phys. Chem. Miner.* 39 (1), 17–25. <https://doi.org/10.1007/s00269-011-0456-x>.
- Wang, L., Kong, A., Chen, B., Ding, H., Shan, Y., He, M., 2005. Direct synthesis, characterization of Cu-SBA-15 and its high catalytic activity in hydroxylation of phenol by H2O2. *J. Mol. Catal. A: Chem.* 230 (1–2), 143–150. <https://doi.org/10.1016/j.molcata.2004.12.027>.

- Wang, T., Yuan, X., Li, S., Zeng, L., Gong, J., 2015. CeO₂-modified Au@SBA-15 nanocatalysts for liquid-phase selective oxidation of benzyl alcohol. *Nanoscale* 7 (17), 7593–7602. <https://doi.org/10.1039/c5nr00246j>.
- Wang, X., Wu, G., Li, J., Zhao, N., Wei, W., Sun, Y., 2007. Selective oxidation of benzyl alcohol catalyzed by Cr (salen) complexes immobilized on MCM-41. *J. Mol. Catal. A: Chem.* 276 (1–2), 86–94. <https://doi.org/10.1016/j.molcata.2007.06.012>.
- Wang, X., Wu, G., Wei, W., Sun, Y., 2010. Solvent-free oxidation of alcohols by hydrogen peroxide over chromium Schiff base complexes immobilized on MCM-41. *Transition Met. Chem.* 35 (2), 213–220. <https://doi.org/10.1007/s11243-009-9316-7>.
- Zapata, P.M.C., Nazzarro, M.S., Parentis, M.L., Gonzo, E.E., Bonini, N.A., 2013. Effect of hydrothermal treatment on Cr-SiO₂ mesoporous materials. *Chem. Eng. Sci.* 101, 374–381. <https://doi.org/10.1016/j.ces.2013.06.041>.
- Zhan, G., Hong, Y., Lu, F., Ibrahim, A.-R., Du, M., Sun, D., Li, J., 2013. Kinetics of liquid phase oxidation of benzyl alcohol with hydrogen peroxide over bio-reduced Au/TS-1 catalysts. *J. Mol. Catal. A: Chem.* 366, 215–221. <https://doi.org/10.1016/j.molcata.2012.09.026>.
- Zhang, L., Zhao, Y., Dai, H., He, H., Au, C., 2008. A comparative investigation on the properties of Cr-SBA-15 and CrOx/SBA-15. *Catal. Today* 131 (1–4), 42–54. <https://doi.org/10.1016/j.cattod.2007.10.017>.
- Zhang, R., Vanover, E., Chen, T.-H., Thompson, H., 2013. Visible light-driven aerobic oxidation catalyzed by a diiron (IV) μ -oxo biscorrole complex. *Appl. Catal. A: General* 464, 95–100. <https://doi.org/10.1016/j.apcata.2013.05.025>.
- Zhao, D., Huo, Q., Feng, J., Chmelka, B.F., Stucky, G.D., 1998. Nonionic triblock and star diblock copolymer and oligomeric surfactant syntheses of highly ordered, hydrothermally stable, mesoporous silica structures. *J. Am. Chem. Soc.* 120 (24), 6024–6036. <https://doi.org/10.1021/ja974025i>.
- Zhou, S., Yang, F., Wang, B., Su, H., Lu, K., Ding, Y., Wang, Y., 2018. Oriented decoration in metal-functionalized ordered mesoporous silicas and their catalytic applications in the oxidation of aromatic compounds. *Catalysts* 8 (2), 80.